

Type I Superconductivity in YbSb₂ Single Crystals

Liang L. Zhao,¹ Stefan Lausberg,² H. Kim,³ M. A. Tanatar,³ Manuel Brando,² R. Prozorov,³ and E. Morosan¹

¹*Department of Physics & Astronomy, Rice University, Houston, TX 77005, USA*

²*Max Planck Institute for Chemical Physics of Solids, 01187 Dresden, Germany*

³*Ames Laboratory and Department of Physics & Astronomy, Iowa State University, IA 50011, USA*

(Dated: November 6, 2018)

We present evidence of type I superconductivity in YbSb₂ single crystals, from DC and AC magnetization, heat capacity and resistivity measurements. The critical temperature and critical field are determined to be $T_c \approx 1.3$ K and $H_c \approx 55$ Oe. A small Ginzburg-Landau parameter $\kappa = 0.05$, together with typical magnetization isotherms of type I superconductors, small critical field values, a strong Differential Paramagnetic Effect (DPE) signal, and a field-induced change from second to first order phase transition, confirm the type I nature of the superconductivity in YbSb₂. A possible second superconducting state is observed in the radiofrequency (RF) susceptibility measurements, with $T_c^{(2)} \approx 0.41$ K and $H_c^{(2)} \approx 430$ Oe.

PACS numbers: 74.25.-q, 74.70.Ad

I. INTRODUCTION

A long held empirical belief has been that type I superconductors are generally elementary metals and metalloids, while the majority of superconducting compounds exhibit type II behavior. Among the vast array of known binary and ternary superconductors, the number of systems with type I superconductivity is notably limited.¹⁻⁷

YbSb₂ was first claimed to be a type I superconductor by Yamaguchi *et al.*⁷, solely based on the shape of one $M(H)$ isotherm at 0.4 K. Subsequently, a limited number of studies of the physical properties of YbSb₂ have been published. Among those, Sato *et al.* reported results of density functional theory (DFT) calculations, resistivity and de Haas-van Alphen measurements, which revealed a quasi-two-dimensional Fermi surface.⁸ Two other brief reports of resistivity under pressure⁹ and NQR measurements¹⁰ indicated that T_c is suppressed under pressure $p = 0.4$ GPa, and that YbSb₂ is likely a weakly coupled s -wave superconductor. Given the scarcity of type I superconducting compounds, and the lack of a thorough characterization of the magnetic and thermodynamic properties of YbSb₂, a detailed analysis of the superconducting ground state in this compound is needed. In this paper, we report results of DC and AC magnetization, heat capacity, resistivity and magnetic penetration depth, confirming the superconducting ground state with $T_c \approx 1.3$ K and $H_c \approx 55$ Oe. A discussion of the superconducting parameters, based on the BCS and Ginzburg-Landau (GL) theories, is also provided. The shape of the $M(H)$ curves and a second to first order phase transition in specific heat below T_c , together with large differential paramagnetic effect (DPE), small critical field H_c and GL parameter $\kappa \ll 1/\sqrt{2}$ provide strong evidence for the type I superconductivity in YbSb₂. Moreover, the RF susceptibility data reveal a possible second superconducting transition with $T_c^{(2)} \approx 0.41$ K and $H_c^{(2)} \approx 430$ Oe.

II. EXPERIMENTAL METHODS

YbSb₂ single crystals were synthesized by flux growth technique, using excess amount of Sb. Elemental Yb (Ames Lab, 99.999%) and Sb (Alfa Aesar, 99.9999%) pieces in an atomic ratio of 1:9 were packed in an Alumina crucible and sealed in a quartz ampoule under partial Ar pressure. The ampoule was heated up to 650 °C, kept at that temperature for four hours, then slowly cooled down to 620 °C, after which the excess flux was removed in a centrifuge. The as-grown crystals were thin plates with a typical dimension of $5 \times 5 \times 0.2$ mm³. A 1:1:1 HCl-HNO₃-H₂O solution was used to remove the remnant flux from the surface of the crystals.

Room temperature powder X-ray diffraction (XRD) measurements were carried out on a Rigaku D/Max diffractometer with Cu K_α radiation and a graphite monochromator. Rietveld analysis was performed to determine the lattice parameters, using the RIETICA software package.¹¹

DC magnetization measurements were performed in a commercial Quantum Design Magnetic Properties Measurement System (QD MPMS) with a He3 insert for temperatures between 0.5 and 2 K. For the plate-like crystals, the shape was assumed to be ellipsoidal, and the demagnetization factor N_d was determined from tabulated values.¹² AC magnetization was measured in a dilution refrigerator, using a standard AC susceptometer consisting of two oppositely wound pick-up coils. An external modulation field of 0.1 Oe and 113.7 Hz was applied in the direction parallel to the crystal plate and data were acquired by a lock-in amplifier. After background subtraction, the phase was shifted according to the excitation frequency. In order to obtain absolute values of the magnetization, the data were matched to the results from the QD MPMS measurements. The imaginary part, χ'' , was set to zero at temperatures above T_c , using an appropriate offset. The offset and the scaling to absolute values were the same for both the temperature and field sweeps.

Heat capacity of YbSb_2 was measured in a QD Physical Property Measurement System (PPMS) with a He3 option, using a thermal relaxation technique. To demonstrate the field dependence of heat capacity, measurements were carried out in a magnetic field applied perpendicular to the crystal plate, with magnitudes ranging from 0 to 90 kOe. Temperature dependent AC resistivity was also measured in the QD PPMS, utilizing a standard four-probe method. The sample was cut into a bar-like shape and four platinum wires were attached to the flat surface using Epo-Tek H20E silver epoxy. An AC current of $i = 0.1$ mA and $f = 1000$ Hz was applied along the in-plane direction and resistivity data were taken during cooling.

In-plane magnetic penetration depth $\Delta\lambda(T)$ was determined using a self-resonating tunnel-diode oscillator (TDR)¹³, operating at 16 MHz with an amplitude of $H_{AC} \approx 10$ mOe, temperatures down to 50 mK and in static magnetic fields up to $H_{DC} = 400$ Oe. The sample was mounted on a sapphire rod with the crystal plate perpendicular to both H_{AC} and H_{DC} . Placing the sample into the inductor causes the shift of the resonant frequency $\Delta f(T) = -G4\pi\chi(T)$, where G is a calibration constant determined by physically pulling the sample out of the coil. With the characteristic sample size R , $\Delta\lambda$ can be obtained from $4\pi\chi = (\lambda/R) \tanh(R/\lambda) - 1$.^{14,15}

III. RESULTS AND DISCUSSION

The powder X-ray diffraction pattern of YbSb_2 is shown in Fig. 1. The pattern was refined using a ZrSi_2 -type orthorhombic structure with space group $Cmcm$ and lattice parameters $a = 4.554$ Å, $b = 16.715$ Å and $c = 4.267$ Å, in good agreement with the previously reported values.¹⁶ A small amount of remnant Sb flux ($\sim 5\%$) was found and is marked by a blue asterisk in Fig. 1.

Fig. 2 shows the temperature dependent DC magnetic susceptibility χ of YbSb_2 , measured in a field H parallel to the crystal plate for $H = 10$ and 20 Oe. The demagnetizing effect has been taken into account by calculating $\chi = \chi_{measured}/(1 - N_d\chi_{measured})$, where $\chi_{measured} = M/H$ is the ratio of the measured magnetization M and the applied magnetic field H . The demagnetization factor N_d is estimated to be 0.07, if we approximate the shape of the plate-like crystal as an ellipsoid.¹² For both zero field cooled (ZFC, solid lines) and field cooled (FC, dashed lines) data, the low temperature susceptibility shows a clear Meissner signal at temperatures below $T_c = 1.25$ K for $H = 10$ Oe. The superconducting volume fraction estimated from the ZFC data at this field value is very close to 100%, indicative of bulk superconductivity. As expected, T_c is suppressed by increasing magnetic field. The DC magnetization isotherms $M(H)$ for $T = 0.5$ and 1.0 K are shown in Fig. 3a, before (solid symbols) and after (open symbols) the demagnetization correction. It is clear that the corrected $M(H)$ curves

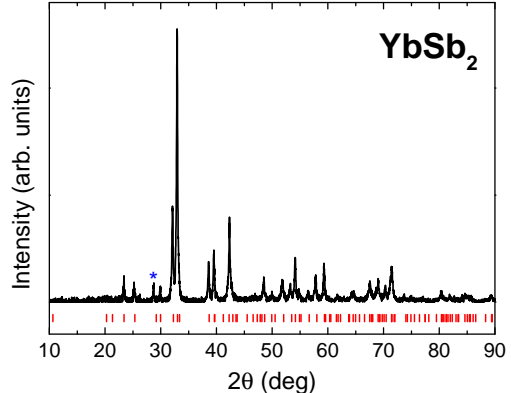


FIG. 1: Powder XRD pattern of YbSb_2 (black line), with peak positions (vertical marks) calculated based on space group $Cmcm$ and lattice parameters $a = 4.554$ Å, $b = 16.715$ Å and $c = 4.267$ Å. A small amount of residual Sb flux is marked by a blue asterisk.

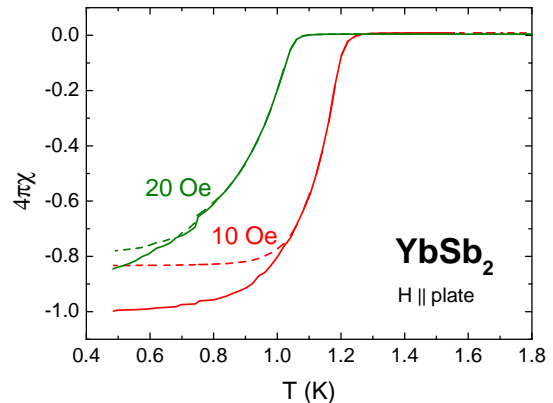


FIG. 2: Temperature dependent susceptibility of YbSb_2 , measured in a DC field parallel to the crystal plate. The ZFC and FC data are plotted as solid and dashed lines, respectively.

show a step-like jump to zero near the critical field, characteristic of type I superconductivity. The full magnetization loops (Fig. 3b) also have the shape typical of type I superconductors.¹⁷⁻¹⁹

The AC susceptibility χ' of YbSb_2 as a function of temperature is shown in Fig. 4. As the field increases from $H = 0$ to 55 Oe, the onset temperature of the Meissner signal drops from 1.41 K to 0.14 K. In a $H = 60$ Oe field, the superconductivity is further suppressed and cannot be detected down to 0.06 K. Similarly, a suppression of H_c with T from 56.3 Oe ($T = 0.06$ K) to 2.3 Oe ($T = 1.28$ K) is illustrated by the $\chi'(H)$ data in Fig. 5. The onset critical temperature T_c and critical field H_c values from AC susceptibility measurements are summarized in a $H - T$ phase diagram in Fig. 10, and will be discussed later. A

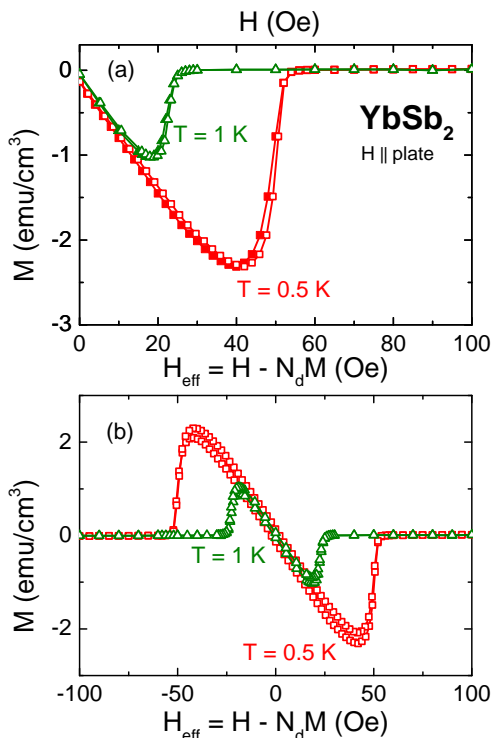


FIG. 3: (a) Isothermal magnetization and (b) full $M(H)$ loops of YbSb_2 for $T = 0.5$ K (squares) and 1 K (triangles) in $H \parallel \text{plate}$. Solid and open symbols correspond to data before (top axis) and after (bottom axis) the demagnetization correction, respectively (see text).

noteworthy feature of the $\chi'(T)$ and $\chi'(H)$ curves is the positive peak in the vicinity of the superconducting transition for $H > 0$, known as the differential paramagnetic effect (DPE) in superconductors.²⁰ The DPE signal originates from the positive $\partial M/\partial H$ values at temperatures right below H_c , and can be observed in either type I or type II superconductors. Nevertheless, since the height of the DPE peak in type II superconductors cannot exceed the absolute value of the diamagnetic susceptibility,⁴ the observed large DPE signal (Figs. 4 and 5) clearly points to type I superconductivity in YbSb_2 .

The field-dependence of the superconducting transition of YbSb_2 is further confirmed by heat capacity measurements in fields up to $H = 90$ kOe. For clarity, a subset of these data are shown in Fig. 6. In the $H = 0$ curve, a clear jump in the heat capacity confirms the bulk superconductivity. The transition temperature T_c , determined at the midpoint of this jump, is close to 1.32 K and agrees well with the previous report.⁷ As H increases, T_c monotonically decreases and drops below 0.4 K (the minimum available temperature for these measurements) at $H = 60$ Oe. The peak at the transition also becomes sharper and higher for $H = 10$ Oe, compared to that for $H = 0$, indicating a change from second to first order phase transition, commonly seen in type I superconductors. As the field is further increased, a non-

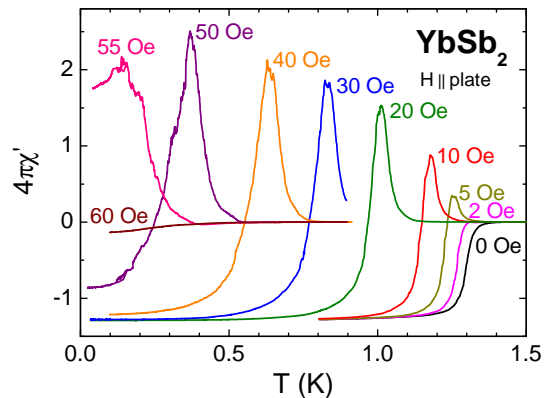


FIG. 4: Temperature dependent AC susceptibility of YbSb_2 , measured in fields H up to 60 Oe.

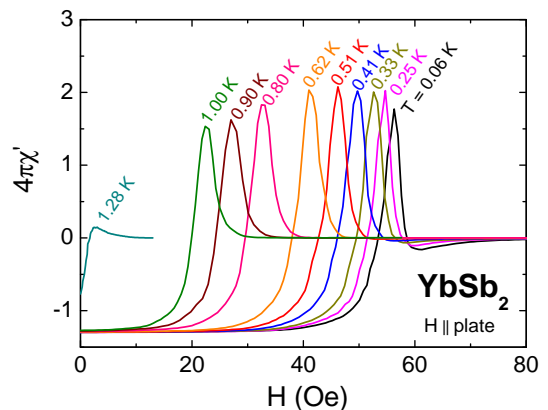


FIG. 5: Field dependent AC susceptibility of YbSb_2 , measured for various temperatures from 0.06 K to 1.28 K.

monotonic change of the electronic and phonon specific heat coefficients γ and β is revealed by the C_p/T vs. T^2 plots (Fig. 6, left inset). While this field dependence remains to be understood, it makes it difficult to determine the electronic specific heat jump $\Delta C_{el} = C_{el,s} - C_{el,n}$ at T_c . An additional difficulty in estimating ΔC_{el} is a possible second superconducting transition at lower temperatures, which will be discussed below. We therefore use the $H = 0$ C_p/T vs. T^2 data (black, Fig. 6, left inset) to estimate γ and β from the linear fit. This gives $\gamma \approx 3.18$ mJ/mol K² and $\beta \approx 0.90$ mJ/mol K⁴. After subtracting the phonon contribution $C_{ph} = \beta T^3$, the jump in the specific heat at the superconducting transition is estimated to be $\Delta C_{el}/\gamma T_c \approx 0.85$ (Fig. 6, right inset), smaller than the BCS value of 1.43. As already mentioned, this could be due to a second superconducting transition and the non-monotonic field dependence of γ and β , as illustrated by a subset of $C_p/T(T^2)$ curves shown in left inset, Fig. 6. The Debye temperature can also be esti-

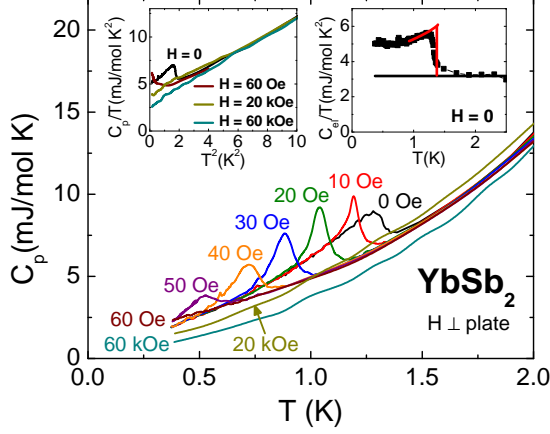


FIG. 6: Temperature dependent heat capacity of YbSb_2 for $H = 0, 10, 20, 30, 40, 50, 60$ Oe and $20, 60$ kOe; left inset: C_p/T vs. T^2 for $H = 0, 60$ Oe, 20 kOe and 60 kOe, showing a field dependent Sommerfeld coefficient γ ; right inset: the superconducting (squares) and normal (black line) electronic specific heat for $H = 0$, plotted as C_{el}/T vs. T . An entropy conservation construct (red lines) is used to determine the jump in the electronic specific heat at T_c .

mated, using $\theta_D = (12\pi^4 N_A r k_B / 5\beta)^{1/3}$, where $r = 3$ is the number of atoms per formula unit. This yields $\theta_D \approx 186$ K.

The AC resistivity of YbSb_2 , for $H = 0$ and $i \parallel \text{plate}$, is shown in Fig. 7. At high temperatures, a linear temperature dependence of $\rho(T)$ is evident, as expected for metals. As seen in the upper inset, the resistivity drops to zero at $T_c = 1.25$ K, with a residual resistivity $\rho_0(2K) = 0.53 \mu\Omega\text{cm}$ just above T_c . The residual resistivity ratio, calculated as $RRR = \rho(300K)/\rho(2K)$, is around 186, indicative of a good quality metal. At temperatures below 8 K and above T_c , the resistivity shows a quadratic dependence on temperature: $\rho = \rho_0 + AT^2$. From a linear fit of $\Delta\rho = \rho - \rho_0$ vs. T^2 , the coefficient A is determined to be $0.0013 \mu\Omega \text{cmK}^{-2}$. The Kadowaki-Woods (KW) ratio $A/\gamma^2 = 12.8a_0$, where $a_0 = 10^{-5} \mu\Omega \text{cm mol}^2 \text{K}^2 \text{mJ}^{-2}$ is a nearly universal value observed in strongly correlated electron systems.²¹ This large KW ratio is consistent with the analogous value previously reported⁸, and could be associated with electron-phonon scattering or enhanced electron correlations.

Based on the resistivity and heat capacity data, several superconducting parameters, such as the London penetration depth λ_L , coherence length ξ , Ginzburg-Landau parameter κ and electron-phonon coupling constant λ_{el-ph} can be estimated. With four formula units per unit cell volume (V), the electron density n of YbSb_2 can be calculated as $n = 8/V = 2.483 \times 10^{-2} \text{\AA}^{-3}$, assuming the valence of Yb to be $2+$. The Fermi wave vector k_F can be roughly estimated if we assume a spherical Fermi surface, which gives $k_F = (3n\pi^2)^{1/3} = 0.903 \text{\AA}^{-1}$.

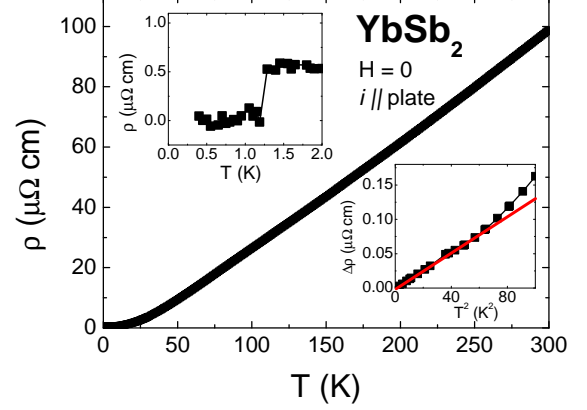


FIG. 7: AC resistivity of YbSb_2 , for $H = 0$ and $i \parallel \text{plate}$. Top inset: a zoomed-in view of the low temperature resistivity around T_c ; bottom inset: $\Delta\rho = \rho - \rho_0$ vs. T^2 (symbols), together with a linear fit (solid line).

The Fermi wave vector k_F , together with the Sommerfeld coefficient $\gamma = 3.18 \text{ mJ/molK}^2 = 6.56 \times 10^{-5} \text{ J/cm}^3 \text{K}^2$, yield the effective electron mass $m^* = \hbar^2 k_F^2 \gamma / \pi^2 n k_B^2 = 1.39 m_0$, where m_0 is the free electron mass. The London penetration depth $\lambda_L(0)$ and coherence length $\xi(0)$ can also be derived as $\lambda_L(0) = (m^*/\mu_0 n e^2)^{1/2} = 40 \text{ nm}$ and $\xi(0) = 0.18 \hbar^2 k_F / k_B T_c m^* = 826 \text{ nm}$. It results that the GL parameter $\kappa = \lambda_L(0)/\xi(0) = 0.05 \ll 1/\sqrt{2}$, confirming the type I superconductivity in YbSb_2 . According to the McMillan theory,²² the electron-phonon coupling is given by

$$\lambda_{el-ph} = \frac{1.04 + \mu^* \ln(\theta_D/1.45T_c)}{(1 - 0.62\mu^*) \ln(\theta_D/1.45T_c) - 1.04}$$

where the Coulomb pseudopotential μ^* is usually between 0.1 and 0.15. Assuming $\mu^* = 0.13$, the electron-phonon coupling is estimated to be $\lambda_{el-ph} \approx 0.51$, suggesting that YbSb_2 is a weakly coupled BCS superconductor. Moreover, the λ_{el-ph} value confirms the effective electron mass m^* as calculated using $m^* = (1 + \lambda_{el-ph})m_0$ which gives $m^* = 1.51m_0$.

Figure 8 shows frequency $\Delta f(T) \sim \chi(T)$ measured for a $0.7 \times 0.5 \times 0.3 \text{ mm}^3$ sample. Data above T_c represent a combination of magnetic and resistive responses in the normal state of YbSb_2 . The skin depth at $T = 1.5$ K was estimated to be $\delta \approx 8.9 \mu\text{m}$, which is much smaller than any dimension of the sample. The skin depth δ was calculated with the residual resistivity $\rho_0 = 0.53 \mu\Omega\text{cm}$ and operating frequency of 16 MHz. A slight upturn before the superconducting transition can be attributed to the response of some paramagnetic impurities. T_c was determined as the temperature where $\Delta f(T)$ deviates from the normal state behavior.

In the pure Meissner state (Fig. 8), for $H_{DC} = 0$, both ZFC and FC curves coincide. Additionally, apart from the superconducting transition, a small feature near 0.11 K was observed, as shown in the inset. This may

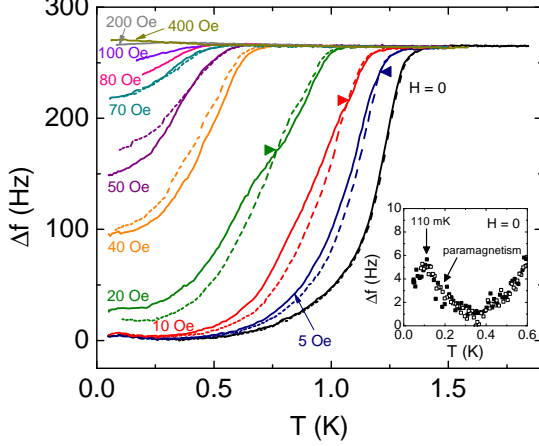


FIG. 8: Shift of resonant frequency $\Delta f = -G4\pi\chi(T)$, measured in fields up to 400 Oe. The ZFC and FC data are shown as solid and dashed lines, respectively; inset: a zoomed-in view of the low temperature data for $H = 0$, with ZFC and FC data shown as solid and open symbols.

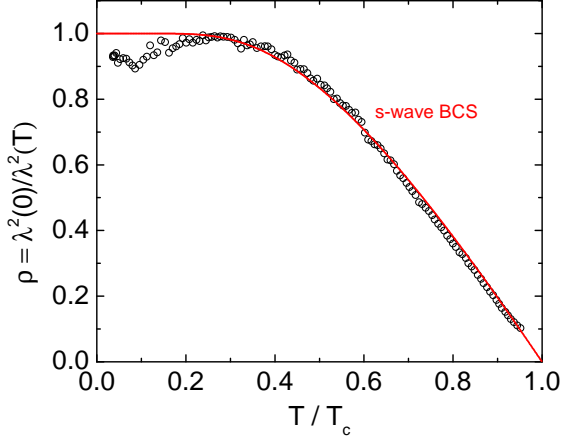


FIG. 9: Superfluid density calculated as $\rho = \lambda^2(0)/\lambda^2(T)$. The solid red line shows a fit to the typical behavior of an s -wave BCS superconductor.

be attributed to a phase associated with extrinsic magnetic impurities. In Fig. 9, the calculated superfluid density, $\rho = \lambda^2(0)/\lambda^2(T)$, is found to be consistent with a single-gap s -wave pairing in YbSb_2 , except for the impurity contribution which modifies the curve at the lowest temperatures. In the presence of magnetic impurities with magnetic permeability $\mu(T)$, the actual measured penetration depth is renormalized as $\lambda_m = \sqrt{\mu(T)}\lambda$, so that the experimentally constructed superfluid density is given by $\rho_m = \lambda^2(0)/[\mu(T)\lambda^2(T)]$. For paramagnetic impurities behaving following the Curie-law, this renormalization leads to a downward trend of ρ_m in the region where real superfluid density is already flat. At higher

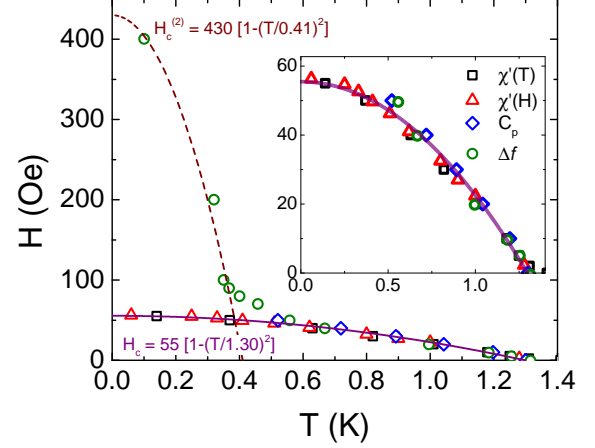


FIG. 10: H - T phase diagram of YbSb_2 . Points determined from $\chi'(T)$, $\chi'(H)$, $C_p(T)$ and $\Delta f(T)$ data are marked by black squares, red triangles, blue diamonds and green circles. The superconductive phase boundary determined from thermodynamic data is illustrated by a purple line. The possible new superconducting state observed in the RF magnetization measurement is marked with a dashed line; inset: a zoomed-in view of the data points from thermodynamic measurements.

TABLE I: Measured and calculated superconducting and thermodynamic parameters of YbSb_2 .

T_c (K)	1.30 ± 0.2
$H_c(0)$ (Oe)	55 ± 2
γ (mJ/mol K ²)	3.18
β (mJ/mol K ⁴)	0.90
θ_D (K)	186
$\Delta C_{el}/\gamma T_c$	0.85
RRR	186
A ($\mu\Omega\text{cm}/\text{K}^2$)	0.0013
A/γ^2 ($10^{-5}\mu\Omega\text{mol}^2\text{K}^2\text{mJ}^{-2}$)	12.8
k_F (\AA^{-1})	0.903
m^* (m_0)	1.45 ± 0.06
$\lambda_L(0)$ (nm)	40
$\xi(0)$ (nm)	826
κ	0.05
λ_{el-ph}	0.51
$T_c^{(2)}$ (K)	0.41
$H_c^{(2)}(0)$ (Oe)	430

temperatures the contribution of paramagnetic impurities rapidly vanishes, since $\mu = 1 + 4\pi\chi = 1 + C/T$, where C is the Curie constant.

In non-zero magnetic field, ZFC-FC Δf curves (Fig. 8) show hysteresis up to $H = 50$ Oe. Interestingly, the FC data indicate stronger repulsion below an intermediate temperature, marked with solid triangles, which systematically decreases with increasing H . This crossover no

longer exists above 40 Oe, and ZFC data recover stronger repulsion. Above 70 Oe, which is greater than H_c determined by various thermodynamic measurements, data still show diamagnetic response without hysteresis, which persists up to 400 Oe. It should also be noted that the AC susceptibility for $H = 60$ Oe (Fig. 4) remains slightly diamagnetic after the DPE peak vanishes, consistent with the results displayed in Fig. 8. The origin of the diamagnetism above the bulk H_c is not clear, however the H - T phase diagram shown in Fig. 10 is reminiscent of a field-dependent pairing state with multiple order parameters in the heavy fermion superconductor $\text{PrOs}_4\text{Sb}_{12}$.^{23,24} More detailed measurements are required to fully understand the rich physics of this unconventional behavior, and to clarify whether this could be bulk or surface superconductivity.

The relationship between T_c and H_c is summarized in the H - T phase diagram (Fig. 10). The H_c values determined from $\chi'(T)$ (squares), $\chi'(H)$ (triangles), C_p (diamonds) and Δf (circles) below ~ 80 Oe can be fit to the expected BCS temperature dependence $H_c(T) = H_c(0)[1 - (T/T_c)^2]$ (solid line, Fig. 10 inset). This gives $H_c(0) = 55$ Oe and $T_c = 1.30$ K. The possible new superconducting state inferred from the RF magnetization (Fig. 8) can also be described with a similar equation $H_c^{(2)}(T) = H_c^{(2)}(0)[1 - (T/T_c^{(2)})^2]$ (dashed line, Fig. 10), which gives $H_c^{(2)}(0) = 430$ Oe and $T_c^{(2)} = 0.41$ K.

The superconducting and thermodynamic parameters of YbSb_2 are summarized in Table I. Several traits of type I superconductors have been observed in this compound, including a small GL parameter $\kappa = 0.05$, typical shape of the DC $M(H)$ isotherms (Fig. 2), a strong DPE signal in the AC magnetization (Fig. 5), small critical field values, and a change from second to first order phase transition induced by magnetic field and visible in specific heat data (Fig. 6). All these observations provide proof of the type I superconductivity in YbSb_2 . In addition, a possible second superconducting state at lower temperatures is observed in RF magnetization (Fig. 8), which reveals unconventional behavior, as of yet not fully understood. This calls for more experiments to elucidate the underlying physics in YbSb_2 .

IV. ACKNOWLEDGMENTS

Work at Rice University was supported by AFOSR MURI. Work at Ames was supported by the U.S. Department of Energy, Office of Basic Energy Sciences, Division of Materials Sciences and Engineering under contract No. DE-AC02-07CH11358. The authors thank Yuri Prots and Juri Grin for help with the structural characterization.

-
- ¹ M. Kobayashi and I. Tsujikawa, *J. Phys. Soc. Jpn.* **50**, 3245 (1981).
² T. T. M. Palstra, G. Lu, A. A. Menovsky, G. J. Nieuwenhuys, P. H. Kes, and J. A. Mydosh, *Phys. Rev. B* **34**, 4566 (1986).
³ U. Gottlieb, J. C. Lasjaunias, J. L. Tholence, O. Laborde, O. Thomas, and R. Madar, *Phys. Rev. B* **45**, 4803 (1992).
⁴ S. Yonezawa and Y. Maeno, *Phys. Rev. B* **72**, 180504(R) (2005).
⁵ V. K. Anand, A. D. Hillier, D. T. Adroja, A. M. Strydom, H. Michor, K. A. McEwen, and B. D. Rainford, *Phys. Rev. B* **83**, 064522 (2011).
⁶ E. Svanidze and E. Morosan, in preparation.
⁷ Y. Yamaguchi, S. Waki, and K. Mitsuoi, *J. Phys. Soc. Jpn.* **56**, 419 (1987).
⁸ N. Sato, T. Kinokiri, T. Komatsubara, and H. Harima, *Phys. Rev. B* **59**, 4714 (1999).
⁹ N. Shirakawa, S. Koiwai, and Y. Uwatoko, *High Pressure Conference of Japan* **10**, 2 (2000).
¹⁰ Y. Kohori, T. Kohara, N. Sato, and T. Kinokiri, *Physica C* **388-389**, 579 (2003).
¹¹ B. Hunter, *International Union of Crystallography Commission on Powder Diffraction Newsletter* p. No. 20 (1998).
¹² J. A. Osborn, *Phys. Rev.* **67**, 351 (1945).
¹³ C. T. V. Degriift, *Rev. Sci. Instrum.* **46**, 599 (1975).
¹⁴ R. Prozorov, R. W. Giannetta, A. Carrington, and F. M. Araujo-Moreira, *Phys. Rev. B* **62**, 115 (2000).
¹⁵ R. Prozorov and R. W. Giannetta, *Supercond. Sci. Technol.* **19**, R41 (2006).
¹⁶ R. Wang, B. R., and H. Steinfink, *Inorg. Chem.* **5**, 1468 (1966).
¹⁷ C. S. Whitehead, *Proc. R. Soc. Lond. A* **238**, 175 (1956).
¹⁸ J. I. Budnick, *Phys. Rev.* **119**, 1578 (1960).
¹⁹ V. F. Kozhevnikov, M. J. VanBael, W. Vinckx, K. Temst, C. VanHaesendonck, and J. O. Indekeu, *Phys. Rev. B* **72**, 174510 (2005).
²⁰ R. A. Hein and J. Raymond L. Falge, *Phys. Rev.* **123**, 407 (1961).
²¹ N. Tsujii, K. Yoshimura, and K. Kosuge, *J. Phys.: Condens. Matter* **15**, 1993 (2003).
²² W. McMillan, *Phys. Rev.* **167**, 331 (1968).
²³ T. Cichorek, A. C. Mota, F. Steglich, N. A. Frederick, W. M. Yuhasz, and M. B. Maple, *Phys. Rev. Lett.* **94**, 107002 (2005).
²⁴ M. Maple, Z. Henkie, W. Yuhasz, P.-C. Ho, T. Yanagisawa, T. Sayles, N. Butch, J. Jeffries, and A. Pietraszko, *J. Magn. Mater.* **310**, 182 (2007).